Hydrol. Earth Syst. Sci. Discuss., 10, 4901–4949, 2013
www.hydrol-earth-syst-sci-discuss.net/10/4901/2013/
doi:10.5194/hessd-10-4901-2013

Hydrology and Earth System Sciences
Open Access
Discussions

How to identify groundwater-caused thermal anomalies in lakes based on multi-temporal satellite data in semi-arid regions

U. Mallast[1,2], C. Siebert[1], R. Gloaguen[2], J. Friesen[3], T. Rödiger[1], S. Geyer[1], and R. Merz[1]

[1]Helmholtz-Centre for Environmental Research, Department Catchment Hydrology, 06120 Halle, Germany
[2]Freiberg University of Mining and Technology, Remote Sensing Group, Institute of Geology, 09599 Freiberg, Germany
[3]Helmholtz-Centre for Environmental Research, Department Computational Hydrosystems, 04318 Leipzig, Germany

Received: 13 February 2013 – Accepted: 7 April 2013 – Published: 18 April 2013

Correspondence to: U. Mallast (ulf.mallast@ufz.de)

Published by Copernicus Publications on behalf of the European Geosciences Union.

Abstract

Information on groundwater discharge over large spatial scales are essential for groundwater management particularly in (semi-) arid regions. If discharge areas are known, direct measurements over larger spatial scales are complicated to obtain by conventional means, why thermal remote sensing is increasingly applied to localize and quantify groundwater discharge. In this context, mostly unconsidered is (i) the influence of surface-runoff that can negatively affect groundwater focused studies and (ii) the representativeness of remotely sensed groundwater discharge based on single thermal images, against the background of discharge intermittency. Addressing these issues we apply a multi-temporal SST data approach based on 19 Landsat ETM+ band 6.2 (high gain) data from the year 2000 until 2002 at the example of the (semi-)arid vicinity of Dead Sea. To be independent of auxiliary rain data we develop a novel approach to identify surface-runoff influenced images solely using image statistics. Compared to foregoing rain events the result reveals a general influence-time of at least two days, but also that a simple time-difference criterion to exclude possible surface-runoff is not advisable. In the second part of the study we evaluate the significance of six statistical measures calculated on a per-pixel basis on the remaining 12 surface-runoff uninfluenced sea-surface-temperature (SST) data using in situ discharge measurements of the Israel Hydrological Service (IHS). We found that the spatial patterns of the standard deviation and range on the SST data series best fit to the IHS observed discharge locations and hence are suitable for detecting groundwater discharge areas.

1 Introduction

Semi-arid regions have a global terrestrial share of the Earth's surface of more than 30 % (Scanlon et al., 2006). Many of these regions exhibit an increasing population number and an expansion of irrigated agriculture areas (Wada et al., 2010). Both facts demand water that due to the nature of semi-arid regions cannot be solely supplied by

HESSD
10, 4901–4949, 2013

surface-water resources but is comprised of up to 50 % by groundwater (Meijerink et al., 2007). This causality requires a sophisticated and sustainable groundwater management that ensures water availability for drinking and irrigation purposes at any time. One important factor in managing groundwater resources is the knowledge of water availability. In a sustainable fashion groundwater availability is derived against the consideration of average annual natural recharge and reduced discharge (Seward et al., 2006). While different methods exist to deduce information on natural recharge over large spatial scales (Scanlon et al., 2002) information on discharge is "complicated due to the fact that direct measurement over large temporal and spatial scales is not possible by conventional means (IAEA, 2007: 1)".

At least for the spatial scale thermal remote sensing offers an opportunity to identify discharge locations. The principle is based on sea-surface temperature SST differences in the uppermost layer (skin layer) of the investigated water body (Donlon et al., 2002; Emery et al., 2001). These differences are affected by atmospheric, bathymetric, anthropogenic or hydrologic (surface and groundwater discharge) processes and result in an array of patterns varying in space and time.

Atmospheric effects on water bodies (lakes, ocean) display a sinusoidal SST course over the seasons reflecting the seasonal variability of air temperature (Nehorai et al., 2009; Wloczyk et al., 2006). The evoked spatio-temporal SST pattern is similar for the entire water body and can even be homogeneous in the case of a water body with uniformly distributed depth. With varying depths and rather complex bathymetry SST patterns become more heterogeneous. Deeper and mostly distal parts exhibit a SST that generally behaves analogous to the air-temperature, but buffers seasonal temperature extremes. Contrastingly, shallow areas follow the temperature extremes as smaller water depths lead to a decreased temperature buffering and hence a general heating (cooling) of these areas in summer (winter) (Baban, 1993).

This homogeneity can be disturbed by local thermal anomalies caused by surface-runoff of rivers (Arnau et al., 2004; Piñones et al., 2005; Walker, 1996), thermal effluents from power plants (Ahn et al., 2006; Xing et al., 2006) and groundwater inflow

HESSD
10, 4901–4949, 2013

(Banks et al., 1996; Danielescu et al., 2009). The caused thermal anomaly in SST patterns remains mostly constant in space and time and is minimally influenced by aforementioned atmospheric or bathymetric factors. While the inflow areas of rivers and power plants are known, groundwater discharge areas are usually unknown. The analysis of the SST pattern anomalies is a promising way to understand and possibly quantify surface and subsurface inflow into water bodies over large spatial scales.

Such SST pattern anomaly analysis are usually based on remotely sensed data where the choice of appropriate spatial and temporal scales is difficult, as discharge zones vary from only a few to several hundred meters in extent. To obtain best possible results, many studies used airborne platforms delivering ground-sampling-distances (GSD) < 1 m that allow the investigation of small scale SST pattern anomalies. The objective of these studies is either to localize groundwater discharge zones based on anomalies (Akawwi et al., 2008; Miller and Ullman, 2004) or to quantify groundwater inflow (Danielescu et al., 2009; Johnson et al., 2008; Roseen, 2002) mostly neglecting a potential surface-runoff. The disadvantage of airborne studies concerns the temporal scale as due to monetary reasons only one moment in time is recorded hindering to analyse temporal variations of temperature patterns.

Contrary to airborne platforms, satellite platforms with thermal sensors contain the great temporal advantage of recording the same location in repeated intervals, where the time period in between recordings varies between several times per day to several days (Sentlinger et al., 2008). This results in numerous images per season and year, which allow a multi-temporal analysis. The multi-temporal analysis is at least in arid regions required because groundwater flow is intermittent (Becker, 2006). A further advantage of satellite data relates to the spatial coverage as typical swath widths range from a few to several hundred kilometres. However, providing this spatial coverage concomitantly pays tribute to GSD, where Landsat ETM+ is the currently best available sensor providing a GSD of 60 m for thermal data (note that data delivered from the United States Geological Survey are resampled to 30 m).

HESSD
10, 4901–4949, 2013

Satellite data applications for groundwater discharge studies are rare. Some studies use single satellite-SST data (MODIS, Landsat ETM+) to localise groundwater discharge locations (Ghoneim, 2008; Wang et al., 2008; Wilson and Rocha, 2012). From these applications only two account for a potential surface-runoff influence and possibly resulting erroneous groundwater discharge detection (Ghoneim, 2008; Wang et al., 2008). Both subjectively exclude certain SST data by assuming a maximum surface-runoff influence time of two days (Ghoneim, 2008) or simply a not further specified selection criterion of no heavy rainfall prior to image recording (Wang et al., 2008). These subjective criteria may not be transferable to other study sites primarily. Secondarily, it requires an accurate and adequate rainfall data basis that specifically in arid regions can be limited (Cohen and Laronne, 2005).

To our best knowledge only the study of Tcherepanov et al. (2005) exploits the multi-temporal advantage of satellite data in an integrative pixel-based manner to identify potential groundwater discharge locations. Given a much smaller seasonal variation in groundwater temperature than in air-temperature and hence in SST, areas with a spatially and temporarily continuous groundwater inflow are expected to show less variation in SST over time. This expectation uses Tcherepanov et al. (2005) and show the SST standard deviation per pixel of a SST series (20 Landsat TM/ETM+ data) to be functional in detecting and amplifying groundwater induced temporal variability patterns. They associate lesser variation with a potential continuous groundwater influence that unfortunately, could not be validated with independent in situ data. However, there multi-temporal approach appears to be promising and highlights the need for a complementary comparison to in situ data and an analysis whether further statistical indicators are similarly practical or even more appropriate to amplify groundwater related thermal anomalies.

The objective of this study is therefore twofold. The first objective concerns the development of an objective and image statistics based approach that compares SSTs off wadi outlets and of the central lake area to differentiate between thermal anomalies caused by groundwater from these caused by surface-runoff. The fulfilment of

HESSD
10, 4901–4949, 2013

this objective overcomes subjectivity of demonstrated approaches in the literature and moreover includes the aspect of transferability to other semi-arid regions. The second objective of this study is to elucidate the performance of different statistical measures calculated on a per-pixel basis within a multi-temporal thermal satellite data approach. In comparison to in situ observations, the result provides an indication of the best-suitable measure in order to identify thermal anomalies that are exclusively related to groundwater discharge.

Both objectives are addressed using the example of the Dead Sea (DS), as it offers different spring types (terrestrial/submarine), spring discharge characteristics (diffuse/concentrated) and ephemeral flash-flood events typical for semi-arid regions.

2 Study area and groundwater inflow

The Dead Sea (DS) is a terminal lake with a currently holomictic regime situated in the Jordan-Dead Sea Graben (Gertman and Hecht, 2002). Along its western shore, groundwaters originate mainly from Cretaceous limy Judea Group and from Quaternary alluvial and limnic coastal aquifers (Yechieli et al., 2010; Mallast et al., 2011). On its eastern flank, groundwater emerge from Jurassic Zerqa and Cretaceous Kurnub sandstone aquifers and the overlaying Upper Cretaceous Ajlun- and Belqa Group (Baaske, 2004; Salameh and Bannayan, 1994). Along the NW shore, groundwater discharges preferentially in Ein Feshkha and Kane/Samar (Fig. 1a and b) with accumulated amounts of 80–150 $\times 10^6$ m^3 a^{-1} (Guttman, 2000; Laronne Ben-Itzhak and Gvirtzman, 2005; Lensky et al., 2005). In general two spring types occur: (i) terrestrial springs emerging along faults or sediment heterogeneities, forming erosion channels due to the lowering of the DS of currently $\sim 1\,m\,a^{-1}$ (Fig. 1c) (Lensky et al., 2005) and (ii) submarine springs that emerge on the lake's bottom in a depth of maximum 30 m (Ionescu et al., 2012), establishing a density driven upward (jet) flow forming a circular pattern on the DS surface (Munwes et al., 2010) (Fig. 1c).

HESSD
10, 4901–4949, 2013

Surface water inputs are limited to the perennial Jordan River discharging 250–300 × 10^6 m^3 a^{-1} (Salameh, 1996) from the north and ephemeral flash-floods generated after significant rainstorms in the rainy season (October–April) (Gertman and Hecht, 2002). The mean annual discharge thereby amounts to 5–27 × 10^6 m^3 a^{-1} with flood volumes of 1–30 × 10^6 m^3 and flow durations of 2–153 h (Greenbaum et al., 2006).

Rainstorms generating flash-floods show temperatures of 10–15 °C (Ayalon et al., 1998), which increase by ∼10 °C until reaching the aquifers. This corresponds to groundwater temperatures in Ein Feshkha, Kane and Samar of 25–28 °C throughout the year (Mazor et al., 1980; Siebert et al., 2011), which become partly heated by ascending brines in places like Qedem and Mineral Beach (Stanislavsky and Gvirtzman, 1999). In contrast, the skin temperature of the DS dynamically varies between 23 °C during winter (December–March) and 30 °C in summer (June–October) with a maximum of > 34 °C in August/September (Gertman and Hecht, 2002). Particularly in summer, the thermal gradient between cool groundwater and warm DS water is promising for thermal analysis of groundwater inflow (Table 1). This fact is even enhanced as fresh to brackish groundwaters (density of 1.06–1.19 g cm^{-3}) ascend to the skin surface of the DS due to the latter's high density (1.24 g cm^{-3}) (Gavrieli et al., 2001).

3 Data and pre-processing

19 Landsat ETM+ band 6.2 (high gain) data (path 174/row 38) covering the years 2000 to 2002 with a cloud cover of less than 15 % are analysed. All data are co-registered to UTM WGS 84 Zone 36N. Although GSD of band 6 is 60 m, all data delivered by the US Geological Survey are resampled to 30 m using cubic convolution (USGS, 2011). Data are recorded at approximately 10:00 local time (GMT+2). To exclude land pixels we apply a threshold of −0.1 of a normalized difference water index (NDWI) derived image using ETM+ band 4 and 2 (see Sect. 4 for details) from the earliest image of the series (15 February 2000).

HESSD
10, 4901–4949, 2013

Band 6.2 of ETM+ data contains recorded thermal radiations from the earth surface within the spectral wavelength of 10.4–12.5 µm. For storing purposes those radiations are converted to an 8-bit dynamic range relating to 256 digital numbers (DN), which need to be re-converted to radiances and subsequently to earth's surface temperatures through different steps, in order to investigate true temperature differences.

The first step re-converts the spaceborne DNs to radiances on top-of-atmosphere (L_{TOA}):

$$L_{TOA} = c_0 + c_1 \mathrm{DN} \tag{1}$$

where c_0 (offset) and c_1 (gain) = radiometric calibration coefficients according to Chander et al. (2009); DN = satellite based digital numbers between 0–255. L_{TOA} consists of thermal radiation leaving the surface and thermal radiation emitted by the atmosphere that both are attenuated by the atmosphere itself. With appropriate knowledge of the atmosphere, a radiative transfer model can be used to estimate the transmission, upwelling and downwelling radiance (Barsi et al., 2005) needed for the calculation of surface radiances for an ideal blackbody (L_T):

$$L_T = \frac{L_{TOA} - L_U - \tau(1-\varepsilon)L_D}{\tau\varepsilon} \tag{2}$$

where ε = surface emissivity; τ = atmospheric transmissivity; L_U = upwelling radiances; L_D = downwelling radiances all for the specific site and time of the respective image.

As we focus on water we apply an emissivity value of 0.97 being aware of the fact that Salisbury and D'Aria (1992) stated water emissivity to alternate between 0.97 and 0.99 in the 8–14 µm region. However, as the DS water contains salt concentrations of $\sim 300\,\mathrm{g\,L^{-1}}$ we follow Wenyao et al. (1987), who found a lower value around 0.97 at higher salinities (> 34 ‰).

Atmospheric transmissivity, as well as upwelling and downwelling radiances are gained for each image through the web-based Atmospheric Correction Tool that is based on MODTRAN (Barsi et al., 2003, 2005). According to the allocated season

HESSD
10, 4901–4949, 2013

of each image we adjust the MODTRAN standard atmosphere to either mid-latitude summer or mid-latitude winter. The required atmospheric profile is selected to be an interpolation for the given centre of the images (Lat 31.8/Lon 35.4) that is subsequently integrated over the selected band 6 spectral response curve. We apply all parameters (Table S1) individually per image into Eq. (2).

To convert surface radiances of an ideal blackbody (L_T) to surface temperatures (T) Planck's radiation law is ETM+ specifically adapted using two pre-launch calibration constants. Solving for T in degree Celsius yields:

$$T\,(^{\circ}\mathrm{C}) = \frac{k_2}{\ln\left(\frac{k_1}{L_T} + 1\right)} \tag{3}$$

where k_1 = calibration constant equal to 666.09 $\mathrm{W\,m^{-2}\,sr^{-1}\,\mu m^{-1}}$); k_2 = calibration constant equal to 1282.71 K after Chander et al. (2009).

According to Barsi et al. (2005) the error of temperature approximation is less than 0.5 ± 0.8 K for the temperature range of 270–330 K. This error indicates the temperature difference due to the application of Planck's radiation law. The absolute error for the present case of the DS is presumably higher since the increased atmosphere of ~ 400 m could not be included in the MODTRAN standard atmospheres.

By using Eq. (3), the skin SST (≤ 1 mm of the uppermost water layer) is calculated, which is about 0.1 K colder than lower water masses due to evaporative heat loss, sensible heat flux and longwave radiation (Wloczyk et al., 2006). For a complete analysis of skin-bulk effects see Donlon et al. (2002).

Besides the satellite data, rainfall data (rain occurrence [date], rain intensity [mm], event duration [d] and accumulated rainfall per event [mm]) for the period 2000–2002 are stored in a database using information from three stations: Gilgal (Lat/Lon 32.00/35.45), Jerusalem (Lat/Lon 31.87/35.22) and Amman (Lat/Lon 31.98/35.98) (Fig. 1). Gilgal belongs to Israel Meteorological Service, while data for the latter two are acquired from Metbroker (http://pc105.narc.affrc.go.jp/metbroker). Since these rainfall

HESSD
10, 4901–4949, 2013

stations cover only the northern part of the DS catchment, we also include daily rain intensities [mm] from Tropical Rainfall Measuring Mission TRMM_3B42 data for completion purposes (Tables S2, S3 and Fig. S1). The used TRMM_3B42 product covers the period from January 2000 to December 2002 with a 3-hourly interval and a spatial resolution of 0.25° (Huffman et al., 2007).

To verify and evaluate inferred groundwater discharge locations, in situ groundwater discharge measurements are available recorded in March 2008 by the Israel Hydrological Service of (IHS).

4 How to separate groundwater from surface-runoff

Direct runoff from flash-floods and groundwater contribute as flowing water fluxes to the Dead Sea. Effectively, a third contribution exists in the form of time-delayed drainage of bank infiltration from alluvial fan gravel. All contributions will influence the SST pattern on the DS and should be visible in the SST data. Several Landsat converted SST data clearly show plume-structures of discharging surface water (bright white colour), which visually exhibit the assumed surface-runoff influence (Fig. 2). At the same time it reveals the necessity to determine and to exclude data influenced by direct runoff from flash-floods or time-delayed bank runoff, if the study intends to investigate groundwater issues. In the following chapter we develop such an approach that is based on the spatial SST variability only, without the need of auxiliary data.

4.1 Theoretical and preliminary considerations

Surface-runoff at the DS is concentrated at wadi outlets. As the runoff flows into the DS two processes take place: (i) within a proximal area the sea surface temperature (SST) pattern of the DS is locally influenced and (ii) inflowing water loses an enormous amount of kinetic energy as it impinges at the standing water body of the DS. Mainly the latter process leads to a spatial limitation of the temperature influence to near-shore

HESSD
10, 4901–4949, 2013

areas, while central parts of the DS remain less influenced at any time. Figure 3 supports this assumption, where it can be seen that the standard deviation of the SST for the central DS area remains steady between 0.2 and 0.4 °C.

Mean SSTs at wadi outlets on the contrary exhibit a wide range that differ to mean SST values of the central area by 6 °C (14 July 2002) in the positive and 2 °C (31 December 2000) in the negative case. Both attribute to aforementioned heating (cooling) processes in shallow environments during summer (winter) periods. We would expect that heating/cooling to affect all shallow areas similarly in the way that they are either uniformly heated during summer or cooled during winter compared to the central area. However, some dates (28 October 2000, 25 June 2001, 18 October 2002 and 19 November 2002) concurrently exhibit heated and cooled shallow environments at wadi outlets compared to the central area mean.

It could be argued that it is simply associated to the statistical variations but when compared to Fig. 2 it is striking that most of these coincide with SST images that show surface-runoff related plume-structures. Consequentially, we conclude that SST differences between central area and areas around wadi outlets probably provide an indication whether surface-runoff occurs or not.

Exploiting only these differences and therefore avoiding auxiliary rainfall information, we create the influence factor (IF), which is a criterion where a simple temperature difference relationship in the form of Eq. (4)

$$\mathrm{IF} = \mathrm{SRT}_k - \mathrm{CAT} \qquad \mathrm{SRT}_1 \ldots \mathrm{SRT}_k \tag{4}$$

where SRT = surface-runoff temperature (k = number of potential discharge points), CAT = central area temperature of the DS serves as indicator, where strong negative IF values represent a surface-runoff influence, whereas values 0 represent explicitly lake related temperatures.

Essential for obtaining thermally observable influences are sufficient temperatures contrasts. For the present case they are given as the absolute temperatures of surface-runoff ($\sim$ 15 °C) are steadily below both the long-term minimum DS temperatures

HESSD
10, 4901–4949, 2013

(23 °C) and also below the coldest measured DS temperatures (16–17 °C) in February 1992 (Ayalon et al., 1998; Gertman and Hecht, 2002).

4.1.1 IF pre-processing

Although temperature differences are demonstrably appropriate to indicate surface-runoff influence a direct linear comparison of SRT and CAT cannot be performed. On the one hand this relates to the continuous retreat of the DS shoreline exposing sediment areas, which differ in heat capacity from water. This characteristic would lead to higher global maximum temperatures of the image and therefore to an erroneous commingling of water- and land-temperatures.

Hence, we introduce a methodical pre-processing (Fig. 4), which accounts for the retreat by defining the land/water interface individually per image using the Normalized Differenced Water Index (NDWI) after McFeeters (1996) (Eq. 5). As threshold we apply a value of −0.2 where values < −0.2 represent water features:

$$\mathrm{NDWI} = \frac{\mathrm{Band4} - \mathrm{Band2}}{\mathrm{Band4} + \mathrm{Band2}} \tag{5}$$

On the other hand, we need to account for seasonal temperature variations that hinder comparing images over an intra- or inter-seasonal basis. With a Max-Min normalisation the comparable basis is created normalising each SST image to $\mathrm{SST_{Norm}}$ (Eq. 6):

$$\mathrm{SST_{Norm}} = \frac{\mathrm{SST_{°C}} - \mathrm{SST_{Min}}}{\mathrm{SST_{Max}} - \mathrm{SST_{Min}}} \tag{6}$$

where $\mathrm{SST_{Norm}}$ = normalised SST image having a value range between 0 and 1, $\mathrm{SST_{°C}}$ = SST pixel in °C, $\mathrm{SST_{Max}}$ = global SST maximum of the SST image, $\mathrm{SST_{Min}}$ = global SST minimum of the SST image.

HESSD
10, 4901–4949, 2013

4.1.2 Definition of SRT and CAT

After pre-processing all images, during this step we define points, where surface-runoff (SR) enters the DS. Each SR originates from crosspoints where the Dead Sea shore, derived from NDWI, intersects with a surface-runoff-path (wadi) calculated by using the eight-direction (D8) flow model. Around each crosspoint, a 1000 m radius was taken as investigation area, defining the SR, which sum up to 19 along the DS. Contrastingly, we assume no influences through surface-runoff and therefore almost steady temperature behaviour in the central area (CA) of the lake. This assumption is supported by Fig. 3 and by findings of Stanhill (1990) and Nehorai et al. (2009), who reported a maximum range of 2.5 °C in the central open sea area. If surface-runoff would thermally impact the CA. the range would be by far greater. Hence, we spatially define the CA by taking a distance of at least 5 km from the actual shoreline orienting on the investigation areas of Stanhill (1990) and Nehorai et al. (2009), who used a distance of ∼ 3–5 km from the shore (Fig. 5).

Applied on the normalised SST images the so obtained 19 SR areas and the CA contain a number of pixels (n) representing normalised temperature values. For SR n varies between 1174 and 2520 depending on the changing shape of the shoreline. For CA n maintains almost constant at around 123 172 (15 February 2000 – first image of the series) and 123 118 (19 November 2002 – last image of the series). Calculating the zonal mean value for each SR and CA results in k representative surface-runoff temperature (SRT) values and one CAT value whose difference (Eq. 4) serves as basis for the evaluation of a surface-runoff influence on the respective image.

4.2 Surface-runoff influence inference through IF

In Fig. 6 the IF of each of the 19 wadi outlets of the DS is plotted against the days after a recorded rainfall event for 19 images. Recalling from Sect. 4.1, strong negative IF values represent a surface-runoff influence. Seven images have only positive values (0.006–0.020). All positive values are explicitly a result of a bathymetrical effect

HESSD
10, 4901–4949, 2013

with higher SSTs of shallow near-shore areas and lower SSTs of the deeper central DS area. Hence, these images are not-surface runoff influenced. Five images exhibit minimum IF values between −0.318 and −0.104. These values clearly indicate surface-runoff influence from a statistical perspective. It is validated by the fact that these images are recorded within the first two days after the end of a rainfall, most likely causing a subsequent surface-runoff event that is also visible in Fig. 2.

Unclear remains the status of the seven images with only minor negative IF values ($-0.1 > x \leq 0$). We expect that beside surface-runoff other factors of natural variability (wind, currents, groundwater, etc.) can lead to slightly lower temperatures. These lower temperatures would also result in small negative IF values, which raises the question of an appropriate threshold to decide whether a surface-runoff influence exists or not.

To solve the question of what negative IF values can occur through natural and surface-runoff independent variability, we calculate the difference between the near-shore temperature (NST) and CAT, similar to the IF analysis. We spatially define NST areas (1000 m radii is maintained to guarantee statistical comparability) to spots along the shore that are at minimum 2000 m away from any wadi outlet to exclude possible drifting of surface-runoff. Analysing the temperature variability of 39 NST areas for the 14 images with minimum IF values of > −0.1 results in 546 observations. The IF values of the 546 observations are grouped to 0.005 classes and plotted against the number of observation in Fig. 7a.

It is apparent that most of the observations have positive values with a maximum around 0.075. This fact clearly shows the bathymetric effect that could be observed before as well. However, it also displays the expected minor negative IF values with a minimum of −0.053 in regions, where no surface-runoff can occur. Hence, it proves that natural variability can cause minor negative values, which can now be quantified to −0.053. IF values below −0.053 are assumed to represent surface-runoff influence and should be excluded for groundwater related studies.

Despite the threshold indication we would like to draw some attention to the number of observations with negative values. Figure 7b shows an enlargement of the negative

HESSD
10, 4901–4949, 2013

fraction of Fig. 7a, where it can be seen that the number of observations per class is small ranging from only 1 to 6 with 6 different images displaying these minor negative IF values. Since this number of observation is comparatively small we presume that not all possible circumstances of natural variability are covered. As the circumstances might differ in other study areas possibly causing a slightly changed IF value we suggest taking the −0.053 threshold as indication and reassess SST images exhibiting an IF value range between −0.053 and 0 visually to ensure the maximum applicable data basis.

4.3 Evaluation of surface-runoff influence time

Sorting the applied SST images after the calculated IF value and comparing it to available rainfall information from rain stations and TRMM_3B42 data indicates an influence through surface-runoff for a minimum of two days after the end of the last day of rain (Fig. 2). This raises two further questions:

1. Is the 2-day-influence time physically feasible and what is the maximum influence time?

2. Is it appropriate to evaluate SST data suitability for groundwater studies using certain influence times?

We address the first question by determining the maximum physically feasible influence time using Darcy's law (Eq. 7). Recalling from Sect. 2 the duration of flash-floods in the DS region is at maximum six days for major rain events (> 20 mm) (Greenbaum et al., 2006). This event follows a time-delayed runoff as water-filled pores in wadi courses and – fans slowly drain. To quantify the longest possible duration of complete "pore-runoff" ($t_{\text{pore-runoff}}$) we assume maximum possible conditions such as pore space to be completely saturated and geometries (volume and trough-flown cross-section) of the largest wadi fan (wadi Darga) along the Dead Sea (see Tables S4 and S5 for a complete description of input parameters and calculation).

HESSD
10, 4901–4949, 2013

$$t_{(\text{pore-runoff})} = V_{\text{total}} \cdot \frac{n_{\text{pores}}}{100} \cdot \left(-\text{kf} \cdot \frac{(h_a - h_b)}{L} \cdot A \right)^{-1} \quad (7)$$

where V_{total} = volume of the alluvial fan [m^3], n_{pores} = porosity of fan material [%], kf = hydraulic conductivity of the fan [$m\,s^{-1}$] h_a and h_b = elevation for start and end point [m], L = length between h_a and h_b, A = cross-sectional area [m^2].

Solving Eq. (7) with given parameters results in 98.6 h (4.11 days), during which stored bank infiltrates from pores of the alluvial fan still drain towards the DS. Adding to this number the maximum flash-flood duration of 6 days returns a maximum influence time of 10 days after the end of a rain event, where it can be assumed that surface-runoff impacts the thermal characteristics of the DS.

Comparing the maximal physical feasible influence time of 10 days to Fig. 6 reveals two facts. On the one hand, that the IF method is valid to identify SST data that are surface-runoff influenced, as all SST data with strong negative IF values fall within the physically maximum feasibility influence time. On the other hand, it answers the second question as it shows that a simple time difference criterion based on additional rain information is problematic to evaluate SST data suitability.

The reason for this statement concerns two cases. The SST data from 8 March 2002 is recorded one day after the last day of rain. Although the short difference to a foregoing rain event suggests a surface-runoff influence neither the minimum IF value of 0.020, nor any visual indication point at a surface-runoff influence. Hence, a strict time difference criterion would exclude this image, although it is thoroughly applicable.

The second case concerns the SST data from 25 June 2001. The time difference of 29 days to the last day of rain tremendously exceeds the maximal physical feasible influence time of 10 days and hence suggests no influence through surface-runoff due to a rainfall event. In contrast the IF value of −0.076 indicates a surface-runoff influence. Due to the unlikeliness of rainfall during June in this region we assume the occurrence of an external factor such as dyke failure or an artificial release of water to be the cause for the IF value, which at least is described by Closson (2005) for the first case.

HESSD
10, 4901–4949, 2013

Both examples demonstrate that it is not appropriate to evaluate SST data suitability using certain influence times as unexpected events cannot be anticipated a priori and suitable data are possibly excluded. Hence, we conclude that:

1. The previously IF derived surface-runoff influence threshold of about −0.053 is valid as SST data exhibiting a lower IF value have a time difference to the end of the last rain that fall well within the physically maximum feasibility influence time of 10 days.

2. In terms of groundwater study suitability, SST data should not be evaluated based on auxiliary rainfall data, but on the image statistics exclusively in order not to include surface-runoff influenced data or to exclude suitable data.

5 How to amplify groundwater signals

Spatially and thermally persistent groundwater inflow is assumed to stabilize the SST at the inflow location against daily and seasonal temperature variabilities in air and hence in the lake water. This causality leads Tcherepanov et al. (2005) to calculate the mean and standard deviation per pixel of 20 SST images to successfully localize potential groundwater inflow in shallow lakes (water depth < 4 m) using the smallest numbers. Groundwater discharge at the DS, like in many other areas of the world, comprises submarine groundwater discharge with emergence-depths down to at least 30 m below the DS level (Ionescu et al., 2012) and river-like groundwater discharge from terrestrial springs. In this context, it is also interesting to establish, (i) whether the approved statistical measures can also be applied to the DS, (ii) whether other statistical indicators can also be used to locate type-independent groundwater discharge and (iii) what each statistical indicator emphasizes concerning groundwater inflow locations.

From a theoretical perspective, a prerequisite for the thermal detection of groundwater is the domination of its temperature on the skin layer of the DS. Considering terrestrial springs the inherited temperature most likely dominates the SST of the water

HESSD
10, 4901–4949, 2013

body it flows into. The reason is the density difference between groundwater (1.06–1.19 g cm^{-3}) and Dead Sea water (1.24 g cm^{-3}) that forms a buoyant layer associated with the groundwater discharge. At the surface and the central parts of the buoyant layer the temperature is largely maintained while a temperature adaption occurs at small scales along the horizontal and vertical density interface due to friction-induced turbulence (O'Donnell, 1993). The temperature retention and the fact that the horizontal extent of the buoyant layer (discharge plume) has a positive relationship to the discharge volume (Ou et al., 2009) leads to the assumption that larger discharge volumes should be thermally identifiable at least for winter and summer months where a maximum temperature contrast exists.

The question whether groundwater temperature with submarine origin can still be traced on the sea-surface is more complex. It is mainly a function of travel time (t) between emergence at the seafloor and sea-surface that can be calculated using Eq. (8) for round buoyant jets (Lee and Chu, 2003).

$$t(z) = z\left(A\left(\frac{\Delta\rho}{\rho_0}\frac{\pi}{4}D^2\omega_0\right)^{\frac{1}{3}}z^{-\frac{1}{3}}\right)^{-1} \quad (8)$$

where t = travel-time [s], z = depth of emergence [m], A = specific dimensionless constant with a value of 4.2 after Pantokratoras (2001), $\Delta\rho$ = difference of densities between DS water and groundwater [g cm^{-3}], ρ_0 = density of DS [g cm^{-3}], D = outlet diameter [m], ω_0 = velocity at outlet [m s^{-1}].

Given is a groundwater velocity and hence the velocity at the outlet of $\sim 10^{-3}$ m s^{-1} (Yechieli et al., 2010). This number presumably represents a minimum as own measurements in open channels exhibit velocities between 10^{-3}–10^{-1} m s^{-1}. Also given are water densities of 1.19 g cm^{-3} as maximum value for brackish groundwater and 1.24 g cm^{-3} for DS water. The only variables are the emergence depth that according to Ionescu et al. (2012) varies up to a depth of 30 m and the outlet diameter. Ionescu et al. (2012) reports shaft diameters of up to 20 m with presumably smaller outlets, but

HESSD
10, 4901–4949, 2013

also seeps with a diameter of 0.2 m. Accounting for these variabilities we calculate the travel-times for varying depths and diameters that represent minimum values as both outlet velocity and density difference can approach larger values (Fig. 8).

Travel-times remain below ≤ 100 s for (i) small outlets (diameter: < 1 m) with a shallow emergence of < 10 m and (ii) for larger outlets (diameter: > 5 m) with an emergence depth of up to 30 m (black colour in Fig. 8). Although these travel-times are only an approximation assuming a constant velocity and neglecting velocity-reducing influence of e.g. lateral deceleration through currents, it gives an indication on the rapidity of groundwater mass transport towards the sea-surface. Within the open water, a stable thermocline that affects the vertical flow exists between April and August in a depth of 25–28 m below the DS-level (Gertman and Hecht, 2002). Consequentially, groundwater that emerges below this depth might be influenced in terms of velocity and heat transfer, but not in the general density-driven vertical flow. Due to the complexity a detailed analysis of velocity fields and heat transfer is beyond the scope of this study. However, because of the short travel-time we suppose the native groundwater temperature does not completely adapt to ambient temperatures. This assumption might not account for small discharge volumes with small outlet diameters at larger emergence depths and for periods of spring and fall, where ΔT approaches zero. In contrast, during winter and summer months ΔT approaches 5–10 °C. We presume that during these times larger discharge volumes that occur at larger outlet diameters, largely maintain native groundwater temperatures until the surface is reached. According to Lee and Chu (2003), as the vertically flowing groundwater reaches the sea-surface, a buoyancy layer forms with a diameter far greater than the original outlet diameter. Hence, it is conceivable that larger discharge volumes are thermally identifiable at least during winter and summer months even on satellite date with coarse GSD.

Against this theoretical background, we follow Tcherepanov et al. (2005) and calcuate the pixel-by-pixel mean (MEAN) and standard deviation (STD) of the 12 SST images, which are not influenced by surface-runoff and compare the results to in situ discharge measurements from the Israel Hydrological Service (IHS). We further extend

HESSD
10, 4901–4949, 2013

these statistical measures by introducing maximum temperature (MAX), minimum temperature (MIN), median (MEDIAN) and temperature range (RANGE) to test, whether these measures can show certain groundwater characteristics that are not captured by MEAN and STD values.

Figure 9 shows a comparison of all applied statistical measures of the multi-temporal SST series and in situ discharge observations for the major spring site Ein Feshkha. The MAX-image exhibits a thoroughly homogenous pattern with just one cooler spot (site A in Fig. 9) with ~28 °C. The spot is directly connected to the shore and spatially coincides with one of the largest terrestrial springs with a discharge volume of 0.2 $m^3 s^{-1}$. Most interestingly is the fact that the other two larger terrestrial springs with discharge volumes of 0.2 and 0.34 $m^3 s^{-1}$ cause only hardly visible thermal anomalies in the MAX-image. The same applies to the MIN-image. Site A is depicted as warmer spot with a temperature of ~21.6 °C which underlines a thermal stabilization over ambient SSTs (< 20 °C). The difference of 6.2 °C between MIN and MAX image of site A indicates an atmospheric influence on the discharge temperature of ±3 °C. It also reveals that the native temperature of the discharge amounts to ~25 °C that could be verified during a field survey in 2011 by means of physically-measured temperatures of 25.2–25.9 °C.

Analogous to the MAX-image the two larger terrestrial springs north of site A are not clearly depicted in the MIN-image. What is visible is a fringe (greenish colour in Fig. 9) with similar MIN-temperatures of 21.6 °C as site A along the shore. This fringe is by ~1 °C warmer than ambient SST and spatially coincides with all IHS measurement locations of spring discharge independent of discharge volumes. Due to this causality the fringe most likely points at discharge locations. Special attention is given to site B. Parallel to site A the MIN-temperature is ~21.6 °C, but unlike site A it is not connected to the shore. Both facts are evidences for a submarine spring with a diameter of some tens of meters similar to picture D in Fig. 1. Although it cannot be verified with observations made at the same time as the investigation period, submarine springs in this region have been repeatedly observed by the Israel Hydrological Service (IHS, 2012).

HESSD
10, 4901–4949, 2013

MEAN and MEDIAN-images neither show significant zones of discharge nor information on location. Hence, both statistical measures seem not to be suitable to infer groundwater information from a multi-temporal analysis. In contrast, the STD-image clearly exhibits the already observed terrestrial spring (site A) and the submarine spring (site B) with expected low STD values. Again it underlines the fact that temperatures of areas steadily influenced by temperature-constant groundwater discharge vary insignificantly (1.9–3.0 °C) over ambient SST. Additionally, it apparently also reflects discharge locations with concentrated but minor discharge volumes ($< 0.2\,m^3\,s^{-1}$) as low STD areas spatially coincide with all IHS spring measurement-locations (e.g. site C). This suggests that using STD-images enables to primarily provide information on discharge location independent of spring type (terrestrial/submarine) and discharge volumes. Secondarily, we assume the areal extent of the low STD values to form additively, where single discharge sites or volumes cannot be distinguished but are accumulated to a connected area instead. Striking is the fact that even south of site C small STD values occur, where no IHS measurement-locations exist. While this fact represents a drawback in terms of a possible false-identification of groundwater discharge it probably results from a steady deflection through wind or Corriolis forces as described by Ou et al. (2009). Another drawback is a noisy transition zone between the low STD value area and the central parts of the DS.

Low values (< 8.5 °C) of the RANGE-image indicate the same discharge locations as the STD images accompanied by less noise in the transition zone and distinguishable discharge sites (e.g. A and C). Striking is that the distinguishable discharge locations spatially exactly match measured discharge locations. This is the case independent of discharge volumes (Fig. 9) including the probable submarine spring (site B). Again, it indicates the expected thermal stabilization through steady groundwater inflow. When comparing the covered area of low range values < 8.5 °C (discharge plume) to spatially according accumulated discharge volumes it even suggests a positive relationship between the discharge plume and the accumulated discharge volume (Table 2).

HESSD
10, 4901–4949, 2013

6 Discussion

The presented approach to identify groundwater discharge into open water bodies encloses a method independent main advantage. It is based on freely available, large scale satellite data sets and thus, represents a considerable alternative over cost and labour intensive field work or airborne campaigns. Only images statistics are incorporated, so that auxiliary information on rainfall that can be scarce and partly do not resolve the high spatio-temporal variability of rainfall in (semi-)arid regions is not required. The multi-temporal SST data analysis allows to infer reliable groundwater discharge locations independent of discharge intermittency. On the other hand, the methodological nature of the approach includes uncertainties that need to be outlined in order to allow a successful application for future studies and to point at further improvements. Hence, the following sections elucidate advantages and uncertainties per processing step of the presented approach.

6.1 Pre-processing of satellite data

The used conversion from digital numbers (DN) to ground-temperatures is widely applied, where different studies could successfully derive ground-temperatures within the expected failure range (e.g. Barsi et al., 2005; Coll et al., 2010). In order to obtain correct ground temperatures an important factor is the emissivity value. We applied an emissivity value of 0.97 as global parameter for saline water in Eq. (2) (Wenyao et al., 1987). Despite the fact that it is justified as the majority of water represents high saline Dead Sea water, a higher emissivity value of 0.99 should be assigned to inflowing, fresher groundwater. This cannot be pursued a priori as it is the intention to identify freshwater influences as a result. However, the 0.02 difference causes a temperature underestimation of 1–1.5 °C (Table 3). This means that for an assumed case of fresher groundwater exhibiting a temperature of 26 °C in nature the conversion into sea-surface temperatures (SST) calculates a temperature of 24.5–25.0 °C. If the SST of the Dead Sea has the same temperature in nature that is maintained during the conversion from

HESSD
10, 4901–4949, 2013

DN into SST, both waters would exhibit identical temperatures in the final SST image. This constellation would impede a differentiation between both waters for the single image case.

This constellation could occur during the periods of spring and fall and hence could play a role. However, since our approach relies on a multi-temporal analysis, where particularly results of the temperature range base on winter and summer contrasts, the emissivity uncertainty most likely does not affect the result. It even evokes the enhancement of the identification of surface-runoff. This is because the temperature of this freshwater input is also underestimated. In turn, this artificially enlarges the temperature contrast to the likewise cooler DS water and enhances the identification of surface-runoff.

Comparing the obtained SST (Fig. 3) to measured SST values of Stanhill (1990) and Gertman and Hech (2002) results in an approximate 2–4 °C difference. This confirms the prior assumption that the enlarged atmosphere increases attenuation of the thermal radiation. While this does not affect the results of the IF nor the multi-temporal analysis as the enlarged atmosphere uniformly influences the entire Dead Sea, it should be noted that the temperature difference corresponds to values given by Stanhill (1990), who reported a difference of 3.0 ± 0.7 °C between satellite derived and measured SST values of the Dead Sea.

6.2 Derivation of IF value

We could show that surface-runoff causes similar thermal anomalies as groundwater discharge (Fig. 2). In order to avoid skewed groundwater related results data that contains surface-runoff need to be excluded. This can be achieved by using time difference criterions (Ghoneim, 2008; Wang et al., 2008). In the case of arid environments this is unfavourable as the often scarce data situation is mostly not capable of adequately reflecting high spatio-temporal variability of rainfall fields. To circumvent this limiting factor the presented IF incorporates only images statistics and hence, represents a

HESSD
10, 4901–4949, 2013

remarkably and autonomously operating alternative to identify surface-runoff influence over the utilization of time difference criterion based on auxiliary rainfall data.

Although the general approach is transferable to other semi-arid study areas, the approach possibly needs to be adjusted. This applies for the IF threshold of −0.053 that depends on temperature differences of surface-runoff and water body. If local temperature gradients differ from the ones presented at the example of the DS the IF threshold might need to be modified individually. An adjustment might also be necessary for the investigation radius of 1000 m around each surface-runoff spot. The chosen radius provided accurate results for the present case, but might vary as e.g. the fluid energy of the runoff or the density differences between runoff and lake water differs significantly. Lower values for these parameters would lead to near-shore influences that would not be detected, if radii are too large.

Another effect that could influence the IF is the mixing of upper and lower water masses in holomictic lakes. The Dead Sea occasionally exhibits this regime (Gertman and Hecht, 2002). After August the onset of cooling and the subsequent density increase causes an overturn where water of the upper strata mix with lower and slightly colder ($>5\,^{\circ}$C) water masses (Gertman and Hecht, 2002). This entails a decreased CAT value which in turn increases the IF value. In short words, if rain falls within the overturn period the IF value approaches a positive value that would misleadingly indicate no rain. However, since rain in late summer is usually uncommon this effect is less relevant for the present case. For groundwater applications in lakes with dimictic or polymictic regimes on the other hand, it has to be strongly considered.

6.3 Amplification of groundwater signals

Groundwater signals from a multi-temporal analysis contain the main advantage of being representative as it encompasses different discharge situations that occur due to the intermittency of groundwater discharge in arid regions (Becker, 2006). It was shown that when calculating range and standard deviation per pixel on an image series, it is possible to identify groundwater discharge locations independent of spring

HESSD
10, 4901–4949, 2013

type (submarine and terrestrial) that could be verified by in situ spring discharge measurements of the Israel Hydrological Service.

Considering the distinguishability of low RANGE values to reflect groundwater discharge plumes, (see RANGE-image in Fig. 9), it was suggested that the horizontal discharge plume area possesses a positive relationship to measured discharge volumes, similar as identified for river discharge by Ou et al. (2009).

Due to the spatial correspondence between in situ measurement locations from the Israel Hydrological Service and the different statistical measures we conclude that: (i) the MAX-image provides information on groundwater discharge location restricted to terrestrial springs with large discharge volumes (ii) the MIN-image behaves similar to the MAX-image but contains the advantage to indicate submarine spring locations and locations of terrestrial springs with small discharge volumes also, (iii) MEAN- and MEDIAN-images are inappropriate since no significant anomalies are visible, (iv) the STD-image outlines all groundwater discharge locations independent of spring type and discharge volume that corresponds to findings of Tcherepanov et al. (2005) and (v) the RANGE-image indicates the same information of groundwater discharge as the STD-image with the advantage to provide distinguishable discharge sites.

The question that arises, and which is important for other study areas, relates to reason for the different behaviours of the statistical measures. The MAX-image depicts exclusively temperatures from the summer period. At the end of the same time the groundwater discharge volume reaches its annual minimum that in turn minimizes the influenced and thermally stabilized area in the Dead Sea (Ou et al., 2009). In parallel rises the air-temperature the native groundwater temperature by $\sim 3\,^{\circ}C$ during the open channel flow sections of the terrestrial springs (see Sect. 5). Due to this reason only the largest spring, which may preserve their outflow temperature, are visible in the MAX-image. This is underlined by Fig. 11 where it can be seen that the maximum values for site B and C (14 July 2002), with assumable (site B) and proven (site C) lower discharge volumes, differ only by $0.3\,^{\circ}C$ to the maximum value for the reference site of the central area. In contrast, the maximum value for site A is $1.7\,^{\circ}C$ lower and additionally shows

HESSD
10, 4901–4949, 2013

a buffered temperature compared to the mean CAT value throughout the entire series. Hence, the MAX-image is only beneficial if high discharge volumes occur, but is of limited use for lower volumes. Promising could also be the identification of thermal groundwater discharge that constantly displays temperatures above the maximum SST of the water body.

In contrast, the MIN-image depicts temperatures from the winter period. The groundwater discharge is highest during that time why the influenced and thermally stabilized areas in the Dead Sea likewise reach a maximum. Unfortunately the temperature contrast approaches a minimum since the groundwater temperature of 25–28 °C is reduced by ∼3 °C through the air-temperature (note that this accounts to the terrestrial springs only where the water temperature is reduced during the open channel flow). As a consequence the resulting temperature of 22–25 °C is almost similar to measured Dead Sea minimum SST of 20–22 °C (Gertman and Hecht, 2002). This causality is also show in Fig. 11. The minimum temperatures of site A and C feature a difference to the CAT of 1.4 °C and 1.1 °C respectively. The minimum temperature of site B is slightly different by 0.8 °C. This is the reason why the MIN-image shows only a fringe (greenish colour) with ∼1 °C warmer temperatures (Fig. 8). The transition from the fringe to distal parts represents a gradual temperature decrease that is hardly visible due to the depicted total temperature-range of 15.2 °C in the MIN-image. These circumstances lead us to the conclusion that the MIN-image is conditionally useful for applications with warmer groundwater temperatures but due to the small differences it should be cautiously applied.

Concerning the detection of groundwater discharge with temperatures of 25–28 °C, both MEAN- and MEDIAN-images have the disadvantage that mean and median SST of the Dead Sea itself amount to similar temperatures as the groundwater discharge. This could have been expected if we take into consideration that the long-term groundwater temperature orientates at the mean air-temperature that in turn governs the SST of the Dead Sea. For the example sites A-C the mean (median) values are 24.9 °C (25.7 °C), 24.9 °C (25.3 °C) and 25.4 °C (26.3 °C) respectively. The central area exhibits

HESSD
10, 4901–4949, 2013

a mean of 24.8 °C and a median of 25.6 °C that proves the above mentioned fact. Therefore, both measures are unadvisable for the identification of groundwater discharge.

STD- and RANGE appear to be better indicators for groundwater discharge that corresponds to findings of Tcherepanov et al. (2005). It originates from the fact that both enhance particularly the small temperature variations that are hardly visible in the MAX- and MIN-images. Figure 10 highlights this relationship as all three example-sites exhibit depleted temperature amplitudes throughout the investigation period. The range (standard deviation) values for the example sites vary from 7.1 °C (2.9 °C) for site A, to 9.5 °C (3.5 °C) and 8.8 °C (3.3 °C) for sites B and C, respectively. The corresponding values for the central area amount to 10.5 °C (4.2 °C).

On the one hand, the constant depletion of SST amplitudes of the example-sites confirms the steady and governing influence through groundwater on the SST. It is to assume that further SST influencing factors such as micrometeorology or water circulation play a role as well. As both are spatially and temporarily inconstant (Hect and Gertman, 2003) the influence is different for individual data and should therefore not dominantly affect the result. SSTs are also subject to bathymetry and sensible/latent heat fluxes that are persistently present factors. However, sensible/latent heat flux is a global parameter that effects the entire sea surface and can thus not affect the identification of groundwater (Fairall et al., 1996). If bathymetry would be the governing force, the SST of the example-sites would by trend exceed the SST values of the central area. In fact, this does only occur for site B at the end of the investigation period. At this special case of site B (submarine discharge) it is interpretable whether the influence decreases over time. This could indicate a dwindling of the discharge volume during summer that consequentially has less effect on the SST at that site.

On the other hand and against the background of identified temperatures at discharge locations, the differently depleted SST amplitudes of the example-sites suggest that the higher the groundwater discharge volume, the slower adapts the native groundwater temperature to ambient Dead Sea temperatures through mixing. In turn, the longer adaption time results in a larger spatial thermal stabilization (discharge plume).

HESSD
10, 4901–4949, 2013

The spatial horizontal dimensions of the discharge plumes roughly correspond to the discharge volumes following a linear relationship between both presented by Ou et al. (2009) among others for river discharge. As the current investigation does not provide sufficient data to prove this relationship it remains as potential and interesting improvement worthwhile for further studies.

7 Conclusions

The complicated situation to gain information on groundwater discharge over large temporal and spatial scales by conventional means (IAEA, 2007) can be facilitated by thermal remote sensing (Meijerink et al., 2007). In this context, the current study presents a multi-temporal SST data approach to identify groundwater discharge locations based on thermal satellite data from Landsat-ETM+. Integrated in the approach is the development of an influence factor that autonomously identifies surface-runoff influenced SST data that would otherwise lead to skewed results. The multi-temporal, pixel-based analysis of surface-runoff unaffected SST data revealed the applicability of statistical measures to identify groundwater discharge locations, evaluated through in situ measurements of spring discharge of the Israel Hydrological Service (IHS). Based on the analysis, we conclude that:

1. Surface-runoff causes similar thermal anomalies as groundwater discharge and needs to be excluded to avoid skewed groundwater related results.

2. The IF represents a remarkably and autonomously operating alternative to identify surface-runoff influence over the utilization of time difference criterion based on auxiliary rainfall data that are mostly not capable of adequately reflecting high spatio-temporal variability of rainfall fields in (semi-) arid areas.

HESSD
10, 4901–4949, 2013

3. It was shown that when calculating range and standard deviation per pixel on a SST data series, it is possible to identify groundwater discharge locations independent of spring type (submarine and terrestrial) that could be verified by in situ spring discharge measurements of the Israel Hydrological Service.

4. Considering the distinguishability of low RANGE values to reflect groundwater discharge plumes, (see RANGE-image in Fig. 9), it was suggested that the horizontal discharge plume area possesses a positive relationship to measured discharge volumes, similar as identified for river discharge by Ou et al. (2009).

The presented study can be used as blueprint for identifying groundwater discharge locations and possibly discharge volumes based on multi-temporal SST data in (semi-)arid environments. Most of all, the free-of-charge Landsat data set represents an interesting and valuable alternative to cost-intensive field work and thermal airborne campaigns to provide information on discharge over large spatial scales that otherwise can be complicated to obtain by conventional means (IAEA, 2007). Although not investigated during the present study the temporal scale can also be addressed when the total available Landsat data set (1984–today) is exploited. This in turn would provide valuable insights under the light of climate change and the need of water and a proper groundwater management for especially (semi-) arid environments.

The proposed approach is not restricted to lakes but also applicable in open water cases. Besides a sufficient temperature contrast an important and so far not mentioned prerequisite for the application of thermal remote sensing data appears to be the density difference between groundwater and water of the lake/ocean it flows into. As mentioned before the density gradient is large for the present case of the DS that most likely alleviates the remotely sensed detection of groundwater. In all cases where groundwater exhibits a smaller density and a temperature contrast compared to the inflowing water body, remotely sensed thermal detection should be feasible. This might also be the case for other climate zones where, however, future research should elucidate individual impacts of e.g. perennial rivers and bathymetry. We furthermore recommend to

HESSD
10, 4901–4949, 2013

seriously consider surface-runoff as additional SST pattern anomaly possibly influencing proper groundwater results. This accounts for singular- and multi-temporal studies and is also platform independent.

Supplementary material related to this article is available online at: http://www.hydrol-earth-syst-sci-discuss.net/10/4901/2013/hessd-10-4901-2013-supplement.pdf.

Acknowledgements. The study was carried out within the frame of the BMBF funded project SUMAR (grant code: 02WM0848). Jan Friesen acknowledges support from the IWAS project (grant code: 02WM1027). We are greatly indebted to Gavriel Weinberger and Udi Galili from the Israel Hydrological Service for providing data on spring discharge, to the Israel National Park Authority and their Ein Feshkha-Kane team who supported us tremendously during field trips and to John Laronne and his group for remarkable patronage of investigations. Moreover, this work was supported by Helmholtz Impulse and Networking Fund through Helmholtz Interdisciplinary Graduate School for Environmental Research (HIGRADE).

The service charges for this open access publication have been covered by a Research Centre of the Helmholtz Association.

References

Ahn, Y.-H., Shanmugam, P., Lee, J.-H., and Kang, Y. Q.: Application of satellite infrared data for mapping of thermal plume contamination in coastal ecosystem of Korea, Mar. Environ. Res., 61, 186–201, doi:10.1016/j.marenvres.2005.09.001, 2006.

Akawwi, E., Al-Zouabi, A., Kakish, M., Koehn, F., and Sauter, M.: Using Thermal Infrared Imagery (TIR) for Illustrating the Submarine Groundwater Discharge into the Eastern Shoreline of the Dead Sea-Jordan, Am. J. Environ. Sci., 4, 693–700, 2008.

HESSD
10, 4901–4949, 2013

Arnau, P., Liquete, C., and Canals, M.: River Mouth Plume Events and their Dispersal in the Northwestern Mediterranean Sea, Oceanography, 17, 22–31, 2004.
Ayalon, A., Bar-Matthews, M., and Sass, E.: Rainfall-recharge relationships within a karstic terrain in the Eastern Mediterranean semi-arid region, Israel: [delta] 18O and [delta]D characteristics, J. Hydrol., 207, 18–31, doi:10.1016/s0022-1694(98)00119-x, 1998.
Baaske, U.: Sequence stratigraphy, sedimentology and provenance of the upper cretaceous siliciclastic sediments of South Jordan, PhD, Faculty for Geo- and Biosciences, University of Stuttgart, Stuttgart, 2004.
Baban, S. M. J.: Detecting and evaluating the influence of water depth, volume and altitude on the variations in the surface temperature of lakes using Landsat imagery, Int. J. Remote Sens., 14, 2747–2758, 1993.
Banks, W. S. L., Paylor, R. L., and Hughes, W. B.: Using Thermal-Infrared Imagery to Delineate Ground-Water Discharged, Ground Water, 34, 434–443, doi:10.1111/j.1745-6584.1996.tb02024.x, 1996.
Barsi, J., Barker, J. L., and Schott, J. R.: An Atmospheric Correction Parameter Calculator for a single thermal band earth-sensing instrument, Proceedings of IGARSS 2003, Centre de Congress Pierre Bandis, Toulouse, France, 2003,
Barsi, J. A., Schott, J. R., Palluconi, F. D., and Hook, S. J.: Validation of a Web-Based Atmospheric Correction Tool for Single Thermal Band Instruments. Earth Observing Systems X, Proc. SPIE Vol. 5882, August 2005, San Diego, CA, 2005.
Becker, M. W.: Potential for Satellite Remote Sensing of Ground Water, Ground Water, 44, 306–318, doi:10.1111/j.1745-6584.2005.00123.x, 2006.
Chander, G., Markham, B. L., and Helder, D. L.: Summary of current radiometric calibration coefficients for Landsat MSS, TM, ETM+, and EO-1 ALI sensors, Remote Sens. Environ., 113, 893–903, doi:10.1016/j.rse.2009.01.007, 2009.
Closson, D.: Structural control of sinkholes and subsidence hazards along the Jordanian Dead Sea coast, Environ. Geol., 47, 290–301, doi:10.1007/s00254-004-1155-4, 2005.
Cohen, H. and Laronne, J. B.: High rates of sediment transport by flashfloods in the Southern Judean Desert, Israel, Hydrol. Process., 19, 1687–1702, doi:10.1002/hyp.5630, 2005.
Coll, C., Galve, J. M., Sanchez, J. M., and Caselles, V.: Validation of Landsat-7/ETM+ Thermal-Band Calibration and Atmospheric Correction With Ground-Based Measurements, IEEE T. Geosci. Remote Sens., 48, 547–555, doi:10.1109/tgrs.2009.2024934, 2010.

HESSD
10, 4901–4949, 2013

Danielescu, S., MacQuarrie, K. T. B., and Faux, R. N.: The integration of thermal infrared imaging, discharge measurements and numerical simulation to quantify the relative contributions of freshwater inflows to small estuaries in Atlantic Canada, Hydrol. Process., 23, 2847–2859, doi:10.1002/hyp.7383, 2009.

Donlon, C. J., Minnett, P. J., Gentemann, C., Nightingale, T. J., Barton, I. J., Ward, B., and Murray, M. J.: Toward Improved Validation of Satellite Sea Surface Skin Temperature Measurements for Climate Research, J. Climate, 15, 353–369, doi:10.1175/1520-0442(2002)015<0353:TIVOSS>2.0.CO;2, 2002.

Emery, W. J., Castro, S., Wick, G. A., Schluessel, P., and Donlon, C.: Estimating Sea Surface Temperature from Infrared Satellite and In Situ Temperature Data, B. Am. Meteorol. Soc., 82, 2773–2785, doi:10.1175/1520-0477(2001)082<2773:ESSTFI>2.3.CO;2, 2001.

Fairall, C. W., Bradley, E. F., Godfrey, J. S., Wick, G. A., Edson, J. B., and Young, G. S.: Cool-skin and warm-layer effects on sea surface temperature, J. Geophys. Res., 101, 1295–1308, doi:10.1029/95jc03190, 1996.

Gavrieli, I., Yechieli, Y., Halicz, L., Spiro, B., Bein, A., and Efron, D.: The sulfur system in anoxic subsurface brines and its implication in brine evolutionary pathways: the Ca-chloride brines in the Dead Sea area, Earth Planet. Sc. Lett., 186, 199–213, doi:10.1016/s0012-821x(01)00247-3, 2001.

Gertman, I. and Hecht, A.: The Dead Sea hydrography from 1992 to 2000, J. Marine Syst., 35, 169–181, doi:10.1016/s0924-7963(02)00079-9, 2002.

Ghoneim, E.: Optimum groundwater locations in the northern United Arab Emirates, Int. J. Remote Sens., 29, 5879–5906, doi:10.1080/01431160801932517, 2008.

Greenbaum, N., Ben-Zvi, A., Haviv, I., and Enzel, Y.: The hydrology and paleohydrology of the Dead Sea tributaries, in: New Frontiers in the Dead Sea Paleoenvironmental Research, edited by: Enzel, Y., Agnon, A., and Stein, M., The Geolgical Society of America, Boulder, CO, USA, 254 pp., 2006.

Guttman, Y.: Hydrogeology of the Eastern Aquifer in the Judea Hills and Jordan Valley, Mekorot, 83 pp., 2000.

Hect, A. and Gertman, I.: Dead Sea Meterological Climate, in: Biodiversity of Cyanoprocaryotes, Algae and Fungi of Israel – Fungal Life in the Dead Sea, edited by: Nevo, O., Oren, A., and Wasser, S. P., Haifa, Israel, 361 pp., 2003.

Huffman, G., Bolvin, D., Nelkin, E., Wolff, D., Adler, R., Gu, G., Hong, Y., Bowman, K., and Stocker, E.: The TRMM Multisatellite Precipitation Analysis (TMPA): Quasi-Global, Multi-

HESSD
10, 4901–4949, 2013

year, Combined-Sensor Precipitation Estimates at Fine Scales, J. Hydrometeorol., 8, 38–55, 2007.
IAEA: Nuclear and isotopic techniques for the characterization of submarine groundwater discharge in coastal zones – Results of a coordinated research project 2001–2006, International Atomic Energy Agency (IAEA)', Vienna, Austria, 192 pp., 2007.
Ionescu, D., Siebert, C., Polerecky, L., Munwes, Y. Y., Lott, C., Häusler, S., Bižić-Ionescu, M., Quast, C., Peplies, J., Glöckner, F. O., Ramette, A., Rödiger, T., Dittmar, T., Oren, A., Geyer, S., Stärk, H.-J., Sauter, M., Licha, T., Laronne, J. B., and de Beer, D.: Microbial and Chemical Characterization of Underwater Fresh Water Springs in the Dead Sea, PLoS ONE, 7, e38319, doi:10.1371/journal.pone.0038319, 2012.
Johnson, A. G., Glenn, C. R., Burnett, W. C., Peterson, R. N., and Lucey, P. G.: Aerial infrared imaging reveals large nutrient-rich groundwater inputs to the ocean, Geophys. Res. Lett., 35, L15606, 15601–15606, doi:10.1029/2008gl034574, 2008.
Laronne Ben-Itzhak, L. and Gvirtzman, H.: Groundwater flow along and across structural folding: an example from the Judean Desert, Israel, J. Hydrol., 312, 51–69, doi:10.1016/j.jhydrol.2005.02.009, 2005.
Lee, J. H. W. and Chu, V.: Turbulent Jets and Plumes – A Lagrangian Approach Kluwer Academics Publishers, Dordrecht, NL, 2003.
Lensky, N. G., Dvorkin, Y., Lyakhovsky, V., Gertman, I., and Gavrieli, I.: Water, salt, and energy balances of the Dead Sea, Water Resour. Res., 41, W12418, doi:10.1029/2005wr004084, 2005.
Mallast, U., Gloaguen, R., Geyer, S., Rödiger, T., and Siebert, C.: Derivation of groundwater flow-paths based on semi-automatic extraction of lineaments from remote sensing data, Hydrol. Earth Syst. Sci., 15, 2665–2678, doi:10.5194/hess-15-2665-2011, 2011.
Mazor, E., Levitte, D., Truesdell, A. H., Healy, J., and Nissenbaum, A.: Mixing models and ionic geothermometers applied to warm (up to 60°C) springs: Jordan Rift Valley, Israel, J. Hydrol., 45, 1–19, doi:10.1016/0022-1694(80)90002-5, 1980.
McFeeters, S. K.: The use of the Normalized Difference Water Index (NDWI) in the delineation of open water features, Int. J. Remote Sens., 17, 1425–1432, doi:10.1080/01431169608948714, 1996.
Meijerink, A. M. J., Bannert, D., Batelaan, O., Lubczynski, M. W., and Pointet, T.: Remote Sensing Applications to Groundwater, IHP-VI, Series on groundwater, 16, United Nations Educational, Scientific and Cultural Organization, Paris, 311 pp., 2007.

HESSD
10, 4901–4949, 2013

Miller, D. C. and Ullman, W. J.: Ecological Consequences of Ground Water Discharge to Delaware Bay, United States, Ground Water, 42, 959–970, doi:10.1111/j.1745-6584.2004.tb02635.x, 2004.
Munwes, Y., Laronne, J. B., Geyer, S., Siebert, C., Sauter, M., and Licha, T.: Direct measurement of submarine groundwater spring discharge upwelling into the Dead Sea, IWRM, Karlsruhe, 2010,
Nehorai, R., Lensky, I. M., Lensky, N. G., and Shiff, S.: Remote sensing of the Dead Sea surface temperature, J. Geophys. Res., 114, C05021, doi:10.1029/2008jc005196, 2009.
O'Donnell, J.: Surface fronts in estuaries: A review, Estuaries and Coasts, 16, 12–39, doi:10.2307/1352761, 1993.
Ou, S., Zhang, H., and Wang, D.-X.: Dynamics of the buoyant plume off the Pearl River Estuary in summer, Environmental Fluid Mechanics, 9, 471–492, doi:10.1007/s10652-009-9146-3, 2009.
Pantokratoras, A.: Effect of ambient temperature on vertical turbulent buoyant water jets, Int. J. Heat Mass Tran., 44, 1889–1898, doi:10.1016/s0017-9310(00)00231-3, 2001.
Piñones, A., Valle-Levinson, A., Narváez, D. A., Vargas, C. A., Navarrete, S. A., Yuras, G., and Castilla, J. C.: Wind-induced diurnal variability in river plume motion, Estuarine, Coastal Shelf Sci., 65, 513–525, doi:10.1016/j.ecss.2005.06.016, 2005.
Roseen, R. M.: Quantifying groundwater discharge using thermal imagery and conventional groundwater exploration techniques for estimating the nitrogen loading to a meso-scale inland estuary, PhD Thesis, University of New Hampshire, New Hampshire, 188 pp., 2002.
Salameh, E. and Bannayan, H.: Water Resources of Jordan – Present Status and Future Potentials, Friedrich Ebert Stiftung Amman, 1994.
Salameh, E.: Water Quality Degradation in Jordan (Impacts on Environment, Economy and Future Generations Resources Base), Friedrich Ebert Stiftung, Royal Society for the Conservation of Nature, Amman, 1996.
Salisbury, J. W. and D'Aria, D. M.: Emissivity of terrestrial materials in the 8–14 [mu]m atmospheric window, Remote Sens. Environ., 42, 83–106, 1992.
Scanlon, B., Healy, R., and Cook, P.: Choosing appropriate techniques for quantifying groundwater recharge, Hydrogeol. J., 10, 18–39, doi:10.1007/s10040-001-0176-2, 2002.
Scanlon, B. R., Keese, K. E., Flint, A. L., Flint, L. E., Gaye, C. B., Edmunds, W. M., and Simmers, I.: Global synthesis of groundwater recharge in semiarid and arid regions, Hydrol. Process., 20, 3335–3370, doi:10.1002/hyp.6335, 2006.

HESSD
10, 4901–4949, 2013

Sentlinger, G. I., Hook, S. J., and Laval, B.: Sub-pixel water temperature estimation from thermal-infrared imagery using vectorized lake features, Remote Sens. Environ., 112, 1678–1688, doi:10.1016/j.rse.2007.08.019, 2008.
Seward, P., Xu, Y., and Brendonck, L.: Sustainable groundwater use, the capture principle, and adaptive management, Water SA, 32, 473–482, 2006.
Stanhill, G.: Changes in the surface temperature of the dead sea and its heat storage, Int. J. Climatol., 10, 519–536, doi:10.1002/joc.3370100508, 1990.
Stanislavsky, E. and Gvirtzman, H.: Basin-scale migration of continental-rift brines: Paleohydrologic modeling of the Dead Sea basin, Geology, 27, 791–794, doi:10.1130/0091-7613(1999)027<0791:bsmocr>2.3.co;2, 1999.
Tcherepanov, E. N., Zlotnik, V. A., and Henebry, G. M.: Using Landsat thermal imagery and GIS for identification of groundwater discharge into shallow groundwater-dominated lakes, Int. J. Remote Sens., 26, 3649–3661, 2005.
Landsat ETM+ product description from the Earth Resources Observation and Science (EROS) Center, available at: https://lta.cr.usgs.gov/LETMP (last access: 17 April 2013), 2011.
Wada, Y., van Beek, L. P. H., van Kempen, C. M., Reckman, J. W. T. M., Vasak, S., and Bierkens, M. F. P.: Global depletion of groundwater resources Geophys. Res. Lett., 37, 1–5, 2010.
Walker, N. D.: Satellite assessment of Mississippi River plume variability: Causes and predictability, Remote Sens. Environ., 58, 21–35, doi:10.1016/0034-4257(95)00259-6, 1996.
Wang, L. T., McKenna, T. E., and DeLiberty, T. L.: Locating Groundwater Discharge Areas in Rehoboth and Indian River Bays and Indian River, Delaware using Landsat 7 imagery, Delaware Geological Survey/University of Delaware, Newark, Delaware, 17, 2008.
Wenyao, L., Field, R., Gantt, R., and Klemas, V.: Measurement of the surface emissivity of turbid waters, Chinese J. Ocean. Limnol., 5, 363–369, doi:10.1007/bf02843818, 1987.
Wilson, J. and Rocha, C.: Regional scale assessment of Submarine Groundwater Discharge in Ireland combining medium resolution satellite imagery and geochemical tracing techniques, Remote Sens. Environ., 119, 21–34, doi:10.1016/j.rse.2011.11.018, 2012.
Wloczyk, C., Richter, R., Borg, E., and Neubert, W.: Sea and lake surface temperature retrieval from Landsat thermal data in Northern Germany, Int. J. Remote Sens., 27, 2489–2502, doi:10.1080/01431160500300206, 2006.

HESSD
10, 4901–4949, 2013

Xing, Q., Chen, C.-Q., and Shi, P.: Method of integrating Landsat-5 and Landsat-7 data to retrieve sea surface temperature in coastal waters on the basis of local empirical algorithm, Ocean Sci. J., 41, 97–104, doi:10.1007/bf03022414, 2006.

Yechieli, Y., Shalev, E., Wollman, S., Kiro, Y., and Kafri, U.: Response of the Mediterranean and Dead Sea coastal aquifers to sea level variations, Water Resour. Res., 46, 12551–12511, W12550, doi:10.1029/2009wr008708, 2010.

HESSD

10, 4901–4949, 2013

Table 1. Temperatures of important waters influencing the thermal pattern of the DS.

Water source	Temperature [°C]	Source
Surface water	10–15	Ayalon et al. (1998)
Groundwater	25–28	Mazor et al. (1980), Siebert et al. (2011)
Dead Sea	23–34*	Gertman and Hecht (2002)

* Lower value represents an average winter temperature, while higher value represents average summer temperature.

HESSD
10, 4901–4949, 2013

Table 2. Example of the effect evoked by conversion from DN to SST with different emissivity values of fresh groundwater in respect to saline DS water.

Emissivity value	DN value (0–255)	Temperature [°C]	Temperature Difference [°C]
0.97	0	−44.0	
0.99	0	−44,2	−0.21
0.97	100	8.6	
0.99	100	7.8	−0.92
0.97	255	58.8	
0.99	255	57.3	−1.49

HESSD
10, 4901–4949, 2013

Table 3. Indication of the relationship between area with range values < 8.5 °C and spatially according accumulated spring discharge volumes measured by the IHS.

Discharge site	Covered area [10^3 m^2]	Accumulated discharge volume [m^3 s^{-1}]	Ratio (Area/Discharge Volume)
A	54	0.43	125
B*	146	1.33	109
C	34	0.31	110

* represents the outlined submarine spring and the adjacent area of connected range values of < 8.5 °C to the southwest of site B.

HESSD
10, 4901–4949, 2013

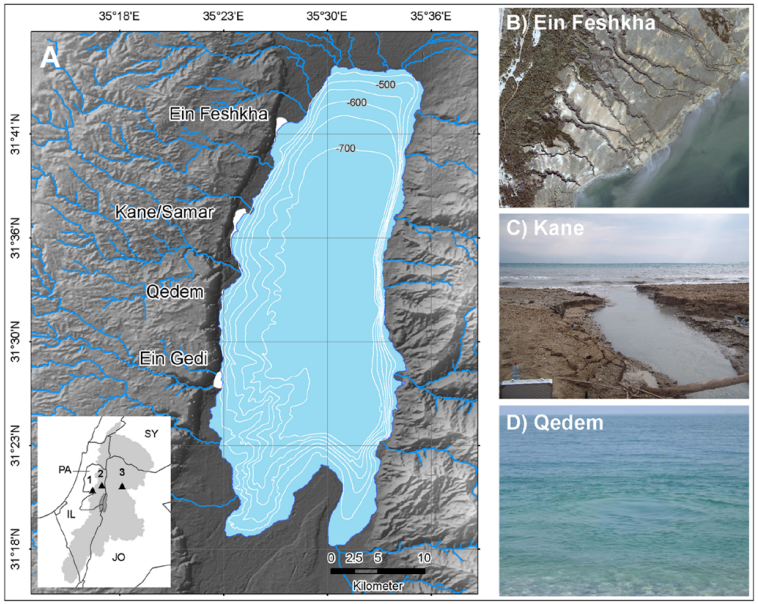

Fig. 1. Study area overview (Map: blue area represents DS in the year 2000; small white areas represent spring areas (Ein Feshkha/Kane/Qedem/Ein Gedi); solid blue lines indicate wadis/river courses; solid white lines indicate 50 m contour lines of the bathymetry after Hall (2000); Subset: grey coloured area represents catchment of the DS; numbers indicate names of climate stations (1 = Jerusalem 2 = Gilgal 3 = Amman); abbrev. IL = Israel PA = Palestine Authorities JO = Jordan SY = Syria); Pictures: all illustrate spring types representative for the study area – **(B)** shows an aerial photograph of the northern Ein Feshkha area from 01/2011 with several erosion channels discharging into the DS; **(C)** shows a similar erosion channel of an upstream located terrestrial spring in the Kane area and **(D)** shows a submarine spring in the Qedem area (source picture **D**: Munwes et al., 2010).

HESSD
10, 4901–4949, 2013

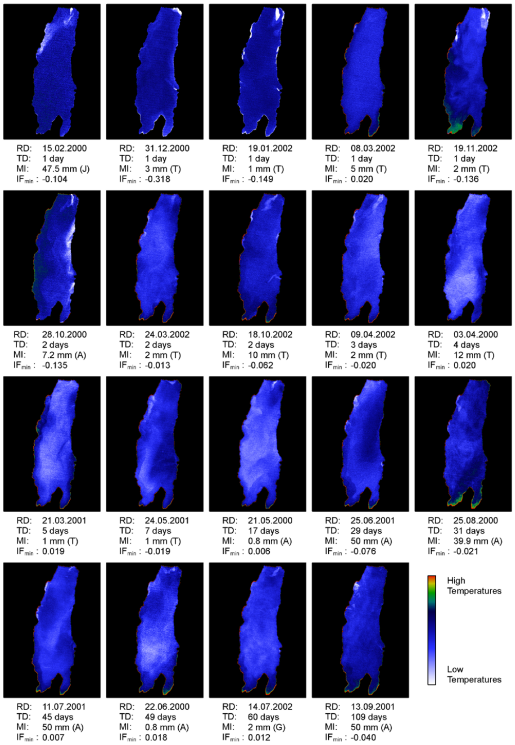

Fig. 2. Overview of available SST data for 2000 until 2002 sorted according to the time difference to the last rain occurrence (data show real temperatures and are individually scaled to enhance the contrast) – RD: date of image recording; TD: Time difference to the end of last rain even; MI: maximum intensity of rain for last rain event; Letter behind MI describes rainfall station, where the last rain event was recorded – J: Jerusalem; G: Gilgal; A: Amman; T: TRMM; IF_{min} = minimum IF value calculated).

HESSD
10, 4901–4949, 2013

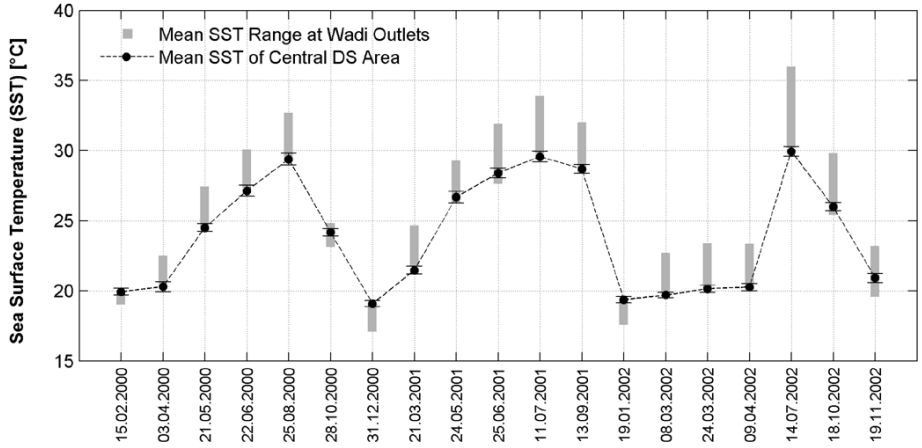

Fig. 3. Mean SST of the central area (CA) of the DS (errorbars represent the standard deviation per date) and the mean SST range of 19 wadi outlets (SR) (see Sect. 4.1.2. for the definition of CA and SR).

HESSD
10, 4901–4949, 2013

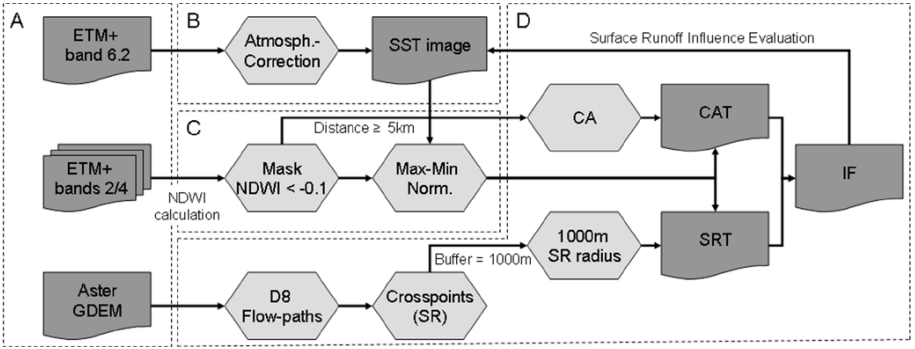

Fig. 4. Flowchart of CAT and SRT derivation for surface-runoff influence identification – dotted line boxes (A): raw data; (B): preprocessing of thermal image; (C): preprocessing for IF calculation; (D): IF calculation.

HESSD
10, 4901–4949, 2013

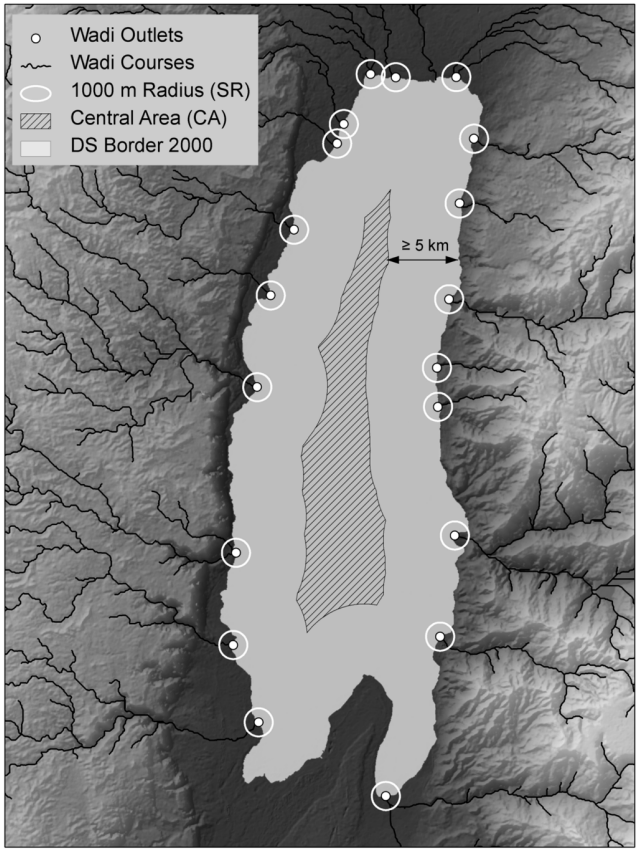

Fig. 5. Wadi outlets and investigated outlet radii respectively that are derived using a simple crosspoint analysis with calculated flow-paths and DS boundary and the derived central area of the DS with a minimum distance of 5 km of any point of the DS boundary.

HESSD
10, 4901–4949, 2013

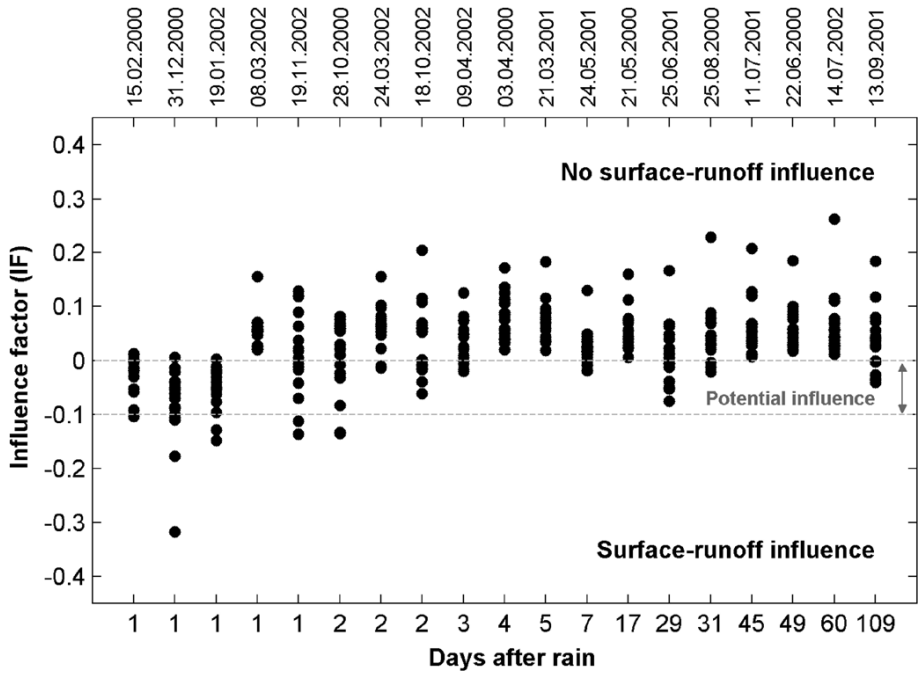

Fig. 6. Difference of the means of **(a)** the normalised temperatures of 19 SRT that represent a surface-runoff area within 1000 m radius areas at the outlet of wadis and **(b)** the normalised temperature of the central area (CAT) of the DS – strong negative values represent a surface-runoff influence while values 0 indicate no surface-runoff influence – the range between −0.1 and 0 regards further analysis as both surface-runoff and influences from wind, currents and groundwater can cause minor negative IF values.

HESSD
10, 4901–4949, 2013

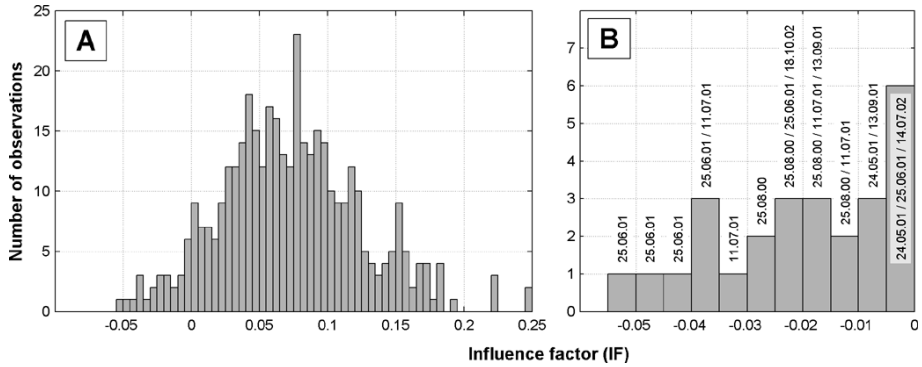

Fig. 7. Difference of the means of **(a)** the normalised temperatures of 39 investigation areas located at least 2000 m away from wadi outlets with a 1000 m radius that represents a natural variability and **(b)** the normalised temperature of the central area (CAT) of the DS – it appears that natural variability can also lead to small negative IF values reaching a minimum value of −0.053 (minimum IF value of the 25 June 2001 image) which hence represents the threshold for differentiation to surface-runoff influenced images.

HESSD
10, 4901–4949, 2013

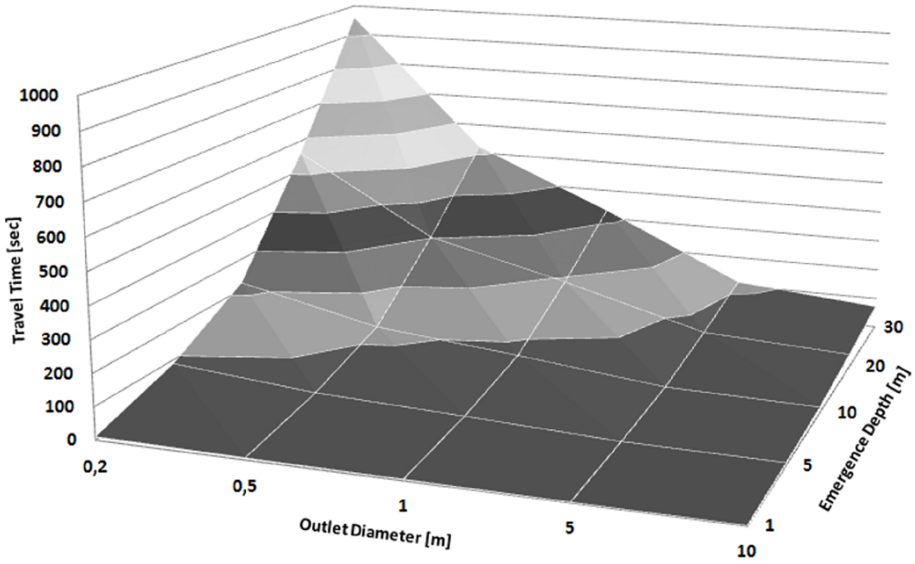

Fig. 8. Travel-times [s] of submarine springs to the sea-surface for varying outlet diameters and emergence depths.

HESSD
10, 4901–4949, 2013

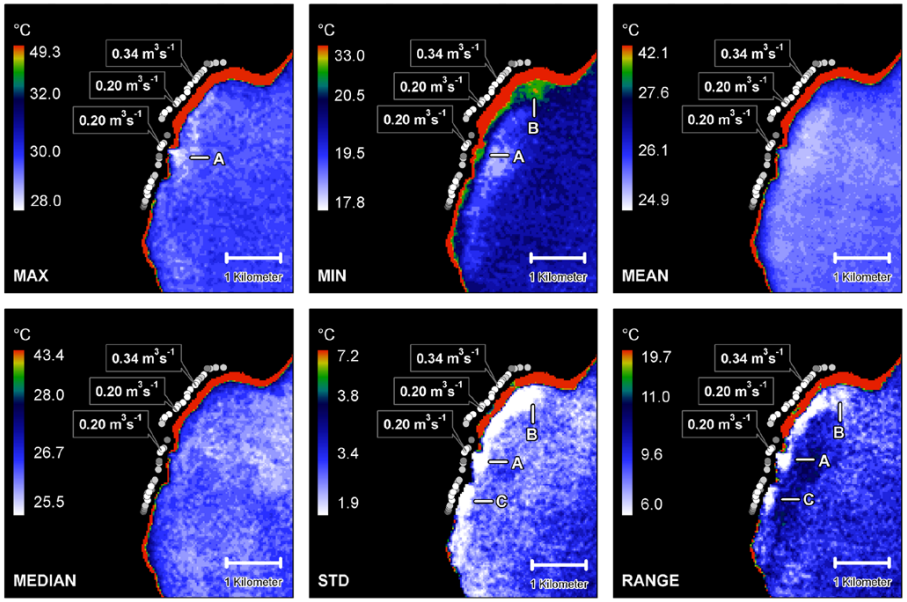

Fig. 9. Intercomparison of statistical measures on a per-pixel basis of a SST data series and in situ measured spring discharge volumes from 03/2008 (white circles $\geq 0.1\,m^3\,s^{-1}$/light grey circles $\geq 0.01 - < 0.1\,m^3\,s^{-1}$/dark grey circles $< 0.01\,m^3\,s^{-1}$) at the example of the major spring site (Ein Feshkha). The tags indicate the discharge volume and the location of the three largest springs at this site – corner-coordinates (lat/lon) of subsets UL 31.72/35.41 LR 31.66/35.50 – note that the measured spring-discharge locations pursued by the IHS are spatially shifted by 200 m perpendicular to the coast to account for the shoreline retreat between the investigation period (2000–2002) and the time of measurement recording.

HESSD
10, 4901–4949, 2013

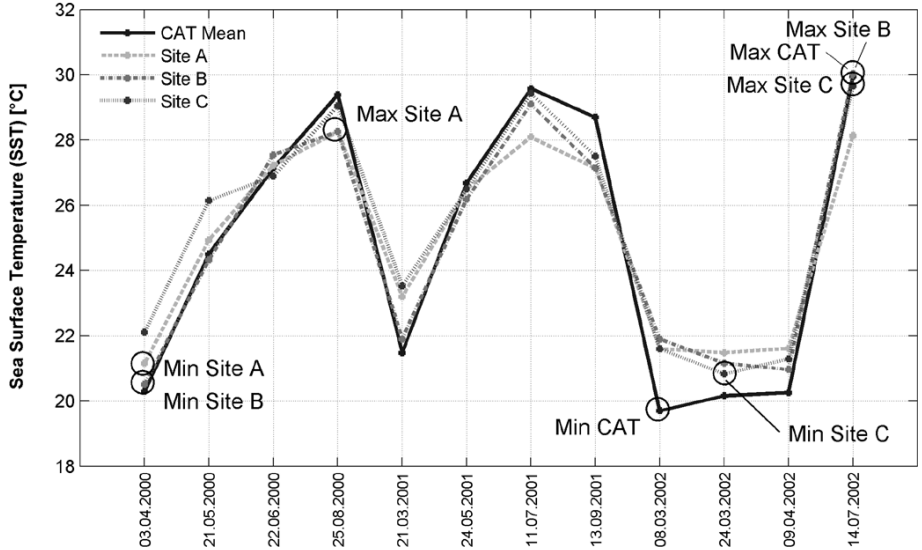

Fig. 10. SST over time for sites A–C and the mean of the central area (CAT) as reference – encircled are the respective minimum and maximum values of each site.

HESSD
10, 4901–4949, 2013